PAPER

Check for updates

Antibacterial, wearable, transparent tannic acid–thioctic acid–phytic acid hydrogel for adhesive bandages†

Xian-hui Shao,[a] Xiao Yang,[b] Yue Zhou,[a] Qing-chang Xia,[a] Yun-ping Lu,[a] Xiao Yan,[a] Chen Chen, [ID] *[a] Ting-ting Zheng,*[a] Lin-lin Zhang,*[a] Yu-ning Ma, [ID] [a] Yu-xia Ma*[a] and Shu-zhong Gao[a]

Making a hydrogel-based first-aid bandage with green resources, desirable biocompatibility, universal adhesive properties, low cost and simple production is a long-standing research aspiration. Considering this, three naturally existing organic acids, namely tannic acid, thioctic acid and phytic acid, were used to construct a novel adhesive gel (TATAPA hydrogel) for epidermal tissue bandage applications. This hydrogel could be synthesized under mild conditions with no need for a freeze–thawing shaping procedure, and was transparent, moldable and stretchable with good stability under continuous water immersion. In lap-shear tests, the TATAPA hydrogel could adhere to various hydrophilic and hydrophobic surfaces. Moreover, in the case of skin tissue adhesion, the hydrogel could be easily peeled off from the skin, meeting wearability requirements. Rheological tests showed that the hydrogel possessed thermal sensitive properties derived from multi-supramolecular interactions. The methicillin-resistant *Staphylococcus aureus* (MRSA)-infected burn wound test demonstrated that the hydrogel had desirable antibacterial activity and was beneficial for wound healing. A femoral artery bleeding assay was also used to reveal that the TATAPA hydrogel could be directly pasted onto the bleeding site for hemostasis. Overall, this hydrogel demonstrates potential as a surgical bioadhesive for a broad range of medical applications.

1. Introduction

Wounds caused by accidental trauma or bacterial infection are an inevitable issue in daily life, often accompanied by bleeding and purulence.[1,2] Common clinical methods such as sutures, staples, and wires are applied to repair large skin defects, causing an unpleasant therapeutic experience for patients as well as an increased risk of secondary infection without the aid of disinfectants or antibiotics.[3–5] Nowadays, researchers find that hydrogels are the best choice for wound healing. Firstly, with a large amount of water retained in their hydrophilic networks, hydrogels can provide a moist environment for wound beds, extracting wound discharge and promoting wound healing.[6–9] Secondly, unlike rubbers, plastic resins or biomacromolecules, hydrogels typically have numerous unique features such as pressure-induced shape regulation, controllable mechanical strength, ideal bio-mimicking properties and accessibility for drug/nanomaterial loading.[10] Thirdly, the crosslinked network of hydrogels is tough enough to avoid excessive swelling or solubilizing under aqueous conditions in practical wound healing procedures.[11–13] Thus far, versatile poly(ethylene glycol)-based,[14] poly(acrylic acid)-based,[15] carbohydrate-based,[16,17] polypeptide-based[18] and poly(vinyl alcohol)-based[19] adhesive gels for wound dressings have been reported by various studies. However, most of the above hydrogels require complicated preparative procedures, accurate chemical design of monomers, toxic crosslinkers or heavy metals and tedious post-synthesis treatment.[11] Although numerous biomacromolecules are recognized as potential green raw material alternatives to synthetic polymers for adhesive hydrogels, they normally face difficulties in creating a standard for the corresponding production because of the varied production places, mutable molecular weights and different extraction methods.[20,21] Moreover, the prevalent application of antimicrobial peptide-based hydrogels is restricted by their high cost and low stability due to proteolytic degradation

[a] *Key Laboratory of New Material Research Institute, Department of Acupuncture-Moxibustion and Tuina, Shandong University of Traditional Chinese Medicine, Jinan 250355, China. E-mail: 21129008@zju.edu.cn, ttz10_10@163.com, linlin66210@outlook.com, myxia1976@163.com*

[b] *The First Affiliated Hospital of Shandong First Medical University (Shandong Qianfoshan Hospital), Jinan 250014, China*

† Electronic supplementary information (ESI) available. See DOI: 10.1039/d2sm00058j
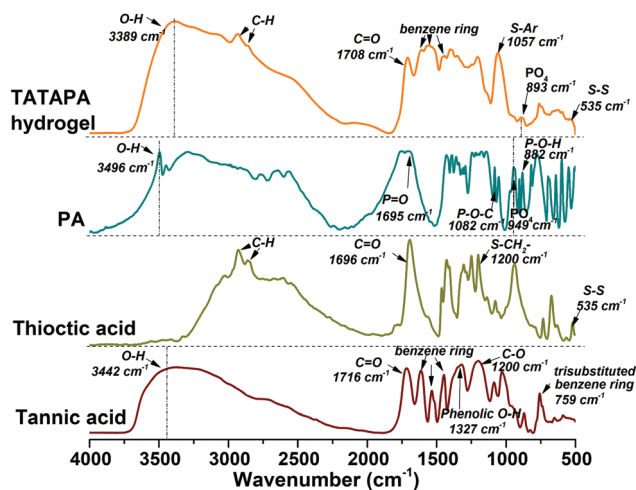
Fig. 1 FT-IR spectra of the TATAPA hydrogel and its raw materials.

and cytotoxicity.[22] Thus, efforts should be made to explore novel hydrogel-based tissue bandages with simple production methods and sustainable resources (Fig. 1).

The bottom-up synthetic method, usually taking advantage of the programmed reactions or self-assembly between functional small molecules, has been employed in the synthesis of functional materials, and examples could be found in click chemistry,[23] metal–phenolic networks,[24] dopamine-based co-deposition,[25] π–π interactions[26] and so on. Hydrogels fabricated using bottom-up protocols integrate the properties of the small molecules involved, making the network design more straightforward and effective compared to bottom-down routes.[27] In consideration of the rising crisis of resource depletion and energy crisis, the combination between the bottom-up method and naturally derived building block is preferable, in which naturally-active small molecules are employed as sustainable monomers and crosslinked in a green manner.[28] As a natural building block, tannic acid is capable of crosslinking other substances either supramolecular or chemically, ensuring an abundant number of functional networks for a large number of applications.[29] Over the latest years, multiple tannic acid-based scaffolds such as bulk hydrogels, films, nanoparticles and nanofibers have been developed by researchers for tissue engineering as well as theranostics.[30,31] For instance, Geng et al. developed a tannic acid–chitosan–phenylboric acid composite hydrogel, which was proved to be an effective hemostatic agent.[32] Mei et al. proposed a series of phenol-metal coating strategies leading to functional films with free radical scavenging and antibacterial properties.[33] Additionally, numerous intermolecular reactions between tannic acid and certain nucleophiles (thiols, amide compounds and amines) belonging to the protein-rich tissue surface render tannic acid-based materials with a long-term skin affinity.[34] Tannic acid is also recognized as an antioxidant, antibacterial, antiviral and anti-inflammatory agent,[35] and is especially appropriate for treating burn wounds and other infected lesions.[36,37] In contrast, though dopamine is extensively used in fabricating tissue adhesives, the high cost, as well as neurological effects, should

not be ignored when it comes to scale-up for industrial production.[38,39] Therefore, tannic acid has advanced advantages in the bottom-up hydrogel design.

Recently, combining the merits of polyphenols and poly(organosulfur) in the hydrogel preparation cuts a striking figure in tissue adhesives for wound healing. The reasons for this combination can be expressed in three aspects: (i) pure polyphenols can hardly form a hydrogel by themselves and need a polymeric spacer to form a highly hydrated network.[40] Coincidentally, poly(organosulfur) derived from thioctic acid can act as a spacer as well as a covalent binder for polyphenols. (ii) The combination between polyphenols and poly(organosulfur) is beneficial for integrating the advantages of antimicrobial,[41] antioxidant,[42] reductive,[43] self-healing,[44] optical[45] and electrochemical properties;[46] (iii) these hybrid hydrogels could be easily prepared under mild conditions, following the rule of green chemistry. Chai et al. reported a novel hydrogel using dopamine and thioctic acid with a strong tissue adhesion force.[47] Tannic acid was used to crosslink thioctic via a polyphenol-thiyl radical Michael addition reaction.[48] However, the resulting hydrogels tended to be amorphous and could not be removed from tissue on demand easily, needing excessive water to wash them off from the skin. Moreover, additional long-term polymerization of dopamine or the free-thawing method was involved in enhancing the stability of the polyphenols–poly(organosulfur) hybrid hydrogel, avoiding gel–sol transition. Therefore, efforts should be made to increase the mechanical reinforcement as well as the comfortable peeling off the performance of the polyphenol–poly(organosulfur) gel system.

Herein, we propose a three-component tannic acid–thioctic acid–phytic acid hydrogel (TATAPA hydrogel) that was synthesized using three commercial feedstocks in a simple, robust, and reproducible method, in which thioctic acid worked as a macromolecular spacer, tannic acid worked as a chemical crosslinker and phytic acid worked as a supramolecular crosslinker. This bottom-up route involved the dissolution of tannic acid, phytic acid and tris base in water, followed by fed-batch addition of thioctic acid for thermal polymerization. The precursor solution could be easily poured into the desired mold, cooled at room temperature overnight for shaping as well as debubbling. Therefore, this method is promising for practical industrial scale-up production without any monomer modification, high energy consumption, harsh reaction conditions, or sophisticated synthetic skills. As a result, this hydrogel integrated multiple functions are derived from polyphenol, poly(organosulfur) and phytic acid-based reinforcement. The chemical structure of the hydrogel network was characterized by Fourier transform infrared (FT-IR) and X-ray photoelectron spectroscopy (XPS) techniques. Basic properties of the hydrogel, including swelling ratio, tensile strength and breaking elongation, were also studied. The adhesive properties were studied by lap-shear tests with various daily used materials as well as by bursting pressure tests. Incorporating multiple dynamic chemical bonds, the hydrogel possessed thermal sensitive performance as indicated by rheological tests. The

in vivo MRSA-infected burn model as well as the *in vivo* rat femoral artery model were employed to assess the practical value of the TATAPA hydrogel in wound healing. Moreover, the biocompatibility, antioxidant activity and biodegradability of TATAPA hydrogel were also evaluated using numerous characterization techniques. Thus, it is our belief that the TATAPA hydrogel could be applied as a first-aid bandage for various epidermal wounds or lesions.

2. Experimental section

2.1. Materials

Tannic acid was purchased from Aladdin Co., Shanghai, China. Tris base (primary standard and buffer, ≥99.9% titration, crystalline) was purchased from Sigma-Aldrich, USA. Phytic acid (PA) was purchased from Zhejiang Dong Jin Biotechnology, Ningbo, China. Thioctic acid (α-lipoic acid) was purchased from Aladdin Co., Shanghai, China. 1,1-Diphenyl-2-picrylhydrazyl (DPPH) was purchased from Macklin Co., Shanghai, China. Dulbecco's Modified Eagle Medium (DMEM) was obtained from Invitrogen (USA). The PBS solution was obtained from Sunshine Bio (Nanjing, China). All other reagents were commercial chemicals and used as received except specially claimed. Ultrapure water (18 MΩ cm resistivity) was also used in the experiments.

2.2. Preparation of thioctic acid–phytic acid (TAPA) hydrogel

First, thioctic acid was fully ground before use. Typically, 1 g tris base and 200 mg PA were dissolved in 5 mL distilled water at 60 °C. Then, 1 g thioctic acid was added to the above solution and the resulting mixture was vortexed for 10 s. A homogeneous solution was obtained after the mixture was stirred at 60 °C for 20 s. Afterward, another 1 g thioctic acid was added and the ultimate mixture was stirred at 60 °C for 1 min to obtain a viscous solution, which could be poured into the desired PP or PTFE molds. The molds were heated to 70 °C for 1 min for deep polymerization and were cooled to room temperature overnight for gelation as well as debubbling. Finally, TAPA hydrogel was obtained as a light-yellow jelly-like substance.

2.3. Preparation of tannic acid–thioctic acid–phytic acid (TATAPA) hydrogel

The preparation procedure was similar to that of TAPA hydrogel. In detail, 1 g tris base, 200 mg PA and a certain amount of

tannic acid (Table 1) were dissolved in 5 mL distilled water at 60 °C for 3 min. Then, 1 g thioctic acid was added to the above solution and the resulted mixture was vortexed for 10 s. A homogeneous solution was obtained after the mixture was stirred at 60 °C for 20 s. Afterwards, another 1 g thioctic acid was added and the ultimate mixture was stirred at 60 °C for 1 min to obtain a viscous solution. The obtained solution was quickly transferred into a syringe and carefully injected into desired PP or PTFE molds. The molds were heated to 70 °C for 1 min for deep polymerization and were cooled to room temperature overnight for gelation as well as debubbling. The obtained TATAPA hydrogel disc or patch could be easily peeled off from the mold underwater. Rhodamine B (Rh B) could be used to stain the TATAPA hydrogel by adding 2 mg of Rh B into the tannic acid–phytic acid–tris base solution at the beginning of the procedure.

2.4. Equilibrium swelling measurements of the TAPA and TATAPA hydrogels

TAPA and TATAPA hydrogels of known weight were freeze-dried and then immersed in distilled water at room temperature until the hydrogel weight remained constant, the excess water on the hydrogel surface was absorbed using a filter paper, and the swollen hydrogel was weighed ($n = 3$). The swelling ratio was calculated using the following formula:

$$\text{Swelling}\% = \left(\frac{m_s - m_d}{m_d} \right) \times 100\%$$

where m_d and m_s are weights of the initial weight of the dried hydrogel and the weight of the swollen hydrogel, respectively.

2.5. Mechanical properties

The hydrogel patches (10 mm width, 60 mm length, 6 mm thickness) were prepared in a PTFE mold. The mechanical properties of the hydrogels were evaluated by a tensile testing machine (Al-3000, GOTECH, Dongguan, China) equipped with a 500 N load cell. The tensile speed was 100 mm min^{-1}. The breaking elongation, the tensile strength of the hydrogels were obtained from the stress–strain curves. Each sample was tested four times.

2.6. Adhesion test

A lap shear test was conducted to assess the adhesive property of the TATAPA hydrogels. In brief, the TATAPA hydrogel patches (25 mm width, 25 mm length, 1 mm thickness) were fixed at 2

Table 1 Ingredients for the synthesis of the TAPA and TATAPA hydrogels

Sample name	Thioctic acid (g)	Tannic acid (g)	Phytic acid (g)	Tris base (g)	Water (mL)	Molar ratio (thioctic acid/tannic acid)	pH[a]
TAPA	2.0	0	0.2	1.0	5	—	6.1
TATAPA-1	2.0	0.2	0.2	1.0	5	80.83	6.0
TATAPA-2	2.0	0.6	0.2	1.0	5	27.71	5.8
TATAPA-3	2.0	1.0	0.2	1.0	5	16.44	5.7
TATAPA-4	2.0	0.6	0.3	1.0	5	27.71	—[b]
TATAPA-5	2.0	0.6	0.2	1.0	4	27.71	—[c]

[a] Denotes that the pH values were measured at 60 °C. [b] Denotes the heterogeneous solution with uncontrollable gelation. [c] Denotes the homogeneous mixture with uncontrollable gelation at 60–70 °C.

For the determination of IL-1β expression *via* immunohistochemistry, the burn wound site samples derived from 1 day and 3 days post-treatment were embedded in paraffin and cut into tissue slices with 5 μm thickness, which were then immersed in xylene for dewaxing. The slices were hydrated in an alcohol gradient for 5 minutes, rinsed using double-distilled water and then subjected to constant shaking three repeated times. Afterwards, the slices were placed in a 0.3% hydrogen peroxide solution, immersed for 30 minutes, and then placed onto a shaking table with double-distilled water three repeated times at room temperature. Considering the antigen repair, a 1% trypsin digestive solution was then applied. After incubation at 37 °C for 20 minutes and successive washing, the slices were soaked in a 1% PBS–bovine serum albumin (BSA, 1%) solution in a humid chamber for 20 minutes at 37 °C. The liquid was removed and the slices were incubated with primary 1L-1β antibody (1 : 200) overnight at 4 °C. On the next day, after washing, the slices were incubated with the corresponding secondary antibody (1 : 200) for 1 h at 37 °C, followed by another washing. Finally, freshly prepared 3′,3′-diaminobenzidine (DAB) substrate was used for dyeing and the development of a brown color was monitored. The slices were rinsed and counterstained with methyl green for 3 minutes followed by washing, dehydration, and neutral gum sealing for observation under a microscope.

2.12 Evaluation of hemostasis of the hydrogels *in vivo*

Male Sprague-Dawley (SD) rats aged 6–8 weeks, weighing approximately 250 g were separated into three groups with each group containing 4 rats. Before the surgery, the anesthesia was performed on rats proceeded using an 8% chloral hydrate solution. The hydrogels were sterilized by ultraviolet irradiation. Sterilization on the glasswares/labware and surgical instruments was either conducted using ethylene oxide or an autoclave. A 2 cm long incision was made on one of the hind legs to expose the femoral artery, which was punctured with a 1 mL syringe needle. Subsequently, a hydrogel patch (10 mm width, 10 mm length, 2 mm thickness) was pasted onto the bleeding site. Bleeding rats without any treatment were used as the blank control. The amount of bleeding out of the hydrogel was measured by weighing the filter paper before and after the surgery. The bleeding time was recorded. The bleeding time was recognized as 10 min if no hemostasis within 10 min.

For the liver hemostasis model of SD rats, once one-quarter of the liver lobe was cut off, and a hydrogel patch (24 mm in diameter, 2 mm thickness) was pasted onto the cut section surface. Then, a clean filter paper with a known mass (M_1) was placed under the liver. The bleeding site without any treatment was used as a negative control, whereas gauze pressing was chosen as a positive control. After 3 minutes of blood flow, the filter paper was stained with blood and re-weighed (M_2). The amount of blood loss was calculated from the mass difference of a filter paper before and after the blood staining: $M_2 - M_1$ ($n = 4$). The hemostatic efficiency for each group was evaluated by the following formula:

$$\text{Hemostatic efficiency} = (M_{\text{blank}} - M_{\text{H}})/M_{\text{blank}} \times 100\%$$

where M_{blank} is the blood loss mass of the negative control, and M_{H} is the blood loss mass of the hemostatic material.

2.13. *In vivo* degradation assay

Nine male SD rats aged 6–8 weeks (200 ± 20 g) were adaptively fed for one week before the experiment. After anesthesia, the backs of the rats were shaved and disinfected using iodine and ethanol. Subsequently, a full-thickness incision (1 cm) was made on each rat. A TATAPA-2 hydrogel disc (5 mm in diameter, 2 mm thickness) was implanted into the subcutaneous tissue. Then, the incision was sutured. Three rats were sacrificed at each time point (day 1, day 3 and day 7) and the implanted sections were analyzed by hematoxylin and eosin (H&E) staining.

2.14. Other characterization methods

Infrared spectra were recorded using a Bruker Tensor-27 IR spectrometer. Field emission scanning electron microscopy (FE-SEM) (Hitachi, S-4800, 15 kV) was used for surface morphology and elemental imaging of the hydrogel patches. The samples for the FE-SEM tests were placed on a tin foil surface and subjected to gold spraying for 60 seconds. X-ray photoelectron spectroscopy (XPS) measurements were carried out using an ESCALAB 250Xi (Thermo Fisher Scientific Inc., USA).

3. Results and discussion

3.1. Hydrogel preparation

The ingredients of the TATAPA hydrogel contained three naturally occurring organic acids including tannic acid, thioctic acid and phytic acid (PA). From the viewpoint of the molecular network structure, this hydrogel was similar to supramacromolecular gels as proposed by Eelkema and Pich,[51] in which tannic acid acted as a covalent crosslinker and phytic acid was used as a non-covalent crosslinker. In our previous study, we verified that tannic acid could crosslink poly(thioctic acid) *via* the polyphenol-thiyl radical Michael addition and the thiyl radical derived from thioctic acid was likely to add to the 3 or 5 aromatic carbons of the pyrogallol group.[48] However, the resulting thioctic acid–tannic acid hydrogel was an amorphous, injectable hydrogel that lacked mechanical strength even after freeze–thawing treatment. With an aim to enhance the mechanical properties as well as the shaping stability, phytic acid-induced hydrogen bonding was introduced since this supramolecular crosslinking method is suitable for multi-hydroxyl polymers such as poly(vinyl alcohol). In the preparation process, fed-batch addition of thioctic acid was necessary to avoid the self-polymerization of thioctic acid as well as the heterogeneous precursor mixture. The added amount of tannic acid ranged from 0 g to 1 g and the final pH of the precursor solution ranged from 5.7 to 6.1 (Table 1). An increased addition amount of PA or decrease in water volume in the wound gives rise to uncontrollable gelation (TATAPA-4 and TATAPA-5 in Table 1). After polymerization at high temperature, TATAPA
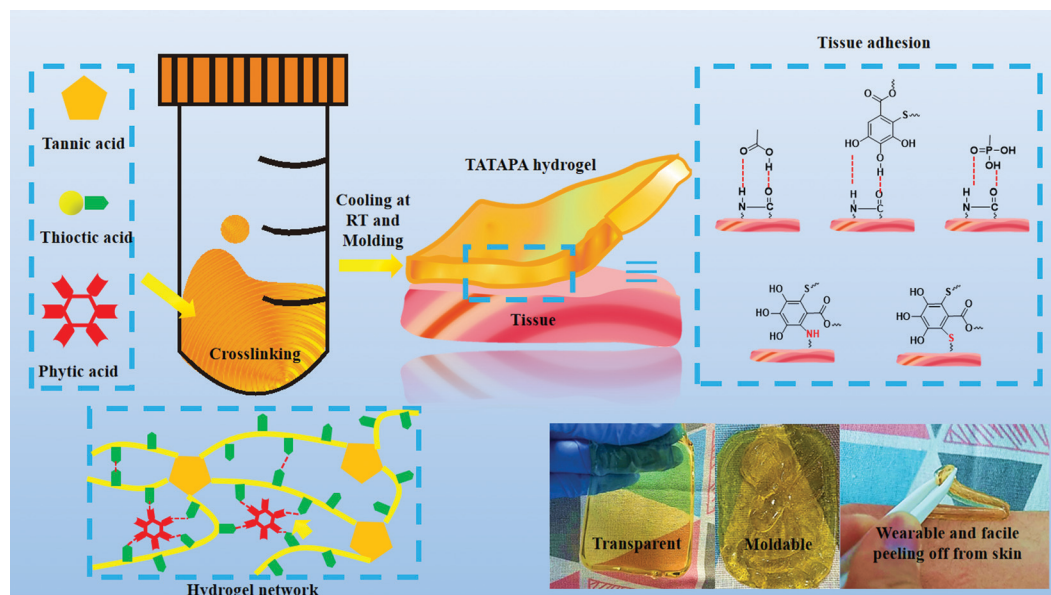
Scheme 1 Preparation of the TATAPA hydrogel, its appearance, macromolecular network and tissue adhesion mechanism.

hydrogels were facile to form the desired shape at room temperature overnight. It should also be noted that the hot precursor solution of TATAPA hydrogel (60–70 °C) maintained excellent fluidity in PP molds rather than PTFE molds. This phenomenon could be explained by the fact that poly(thioctic acid) could form high-density of hydrogel bonds with fluorine atoms of PTFE. Moreover, the precursor solution was hydrophilic, limiting the surface spreading and gap-filling capabilities on PTFE molds. In contrast, with PP containing elements or chemical bonds with weak electronegativity, the supramolecular interactions between the TATAPA precursor solution and PP surfaces were negligible. Thus, this solution could spread out slowly on the PP surface.[28] Therefore, the precursor solution could be directly poured into PP molds followed by standing to remove bubbles. In the case of hydrogel shaping in PTFE molds, the precursor solution should be transferred to a syringe right after polymerization and carefully injected into the molds for debubbling. The obtained TATAPA hydrogel was brown, transparent, shape-stable, wearable and could be easily peeled off from the skin. There is no requirement for tedious modification methods, narrow stoichiometric dosage, or further purification treatment to prepare the TATAPA hydrogel. Considering the low cost of the raw material, mild polymerization conditions and simple preparation process, the TATAPA hydrogel is promising for scale-up production (Scheme 1). The increased tannic acid/thioctic ratio to 1/2 would result in a loss of transparency. In contrast, without the addition of tannic acid, TAPA hydrogel was obtained as a light yellow, soft supramolecular hydrogel (Fig. S1, ESI†).

3.2. Basic characterization of TATAPA hydrogels

The fundamental properties including chemical structure, swelling ratio, tensile strength were studied through multiple measurements. The FT-IR spectrum of the TATAPA hydrogel

showed that a new adsorption peak at 1057 cm^{-1} is assignable to thiophenol (S–Ar) presented, which revealed that thioctic acid crosslinked with tannic acid. Other adsorption peak at 1708 cm^{-1} could be assigned to carbonyl groups. Multiple peaks at 1607, 1554 and 1442 cm^{-1} were corresponding to phenyl residues originating from tannic acid. Aliphatic C–H at 2932, 2859 cm^{-1} and disulfide bond at 535 cm^{-1} could be attributed to the main skeleton of poly(thioctic acid). In contrast to the FT-IR spectrum of PA, the hydroxyl groups of the TATAPA hydrogel shifted to low wavenumbers from 3496 cm^{-1} to 3389 cm^{-1}. Moreover, the adsorption peak of the phosphate group also shifted to low wavenumbers from 949 cm^{-1} to 893 cm^{-1}, which indicated PA-induced hydrogen bonding with tannic acid–thioctic acid hydrogel network during the hydrogel preparation.[52] S2p survey of XPS results showed a disulfide peak at 164.3 eV, an aliphatic organosulfur peak at 163.0 eV, and a thiophenol peak at 163.7 eV in TATAPA hydrogel (Fig. S2a, ESI†). Furthermore, the C1s survey demonstrated the presence of the carbonyl carbon at 288.4 eV, polyphenyl carbon at 286.1 eV and aliphatic carbon at 284.5 eV (Fig. S2b, ESI†). Scanning electron microscopy (SEM) demonstrated that the surface morphology of the hydrogel was smooth without holes (Fig. S3a and b, ESI†). Therefore, it could be concluded that the hydrogel had low swelling performance. Additionally, energy-dispersive spectroscopy mapping revealed that the elements C, O, S, P and N were uniformly distributed throughout the TATAPA hydrogel (Fig. S3c–h, ESI†).

To evaluate the stability under continuous water immersion, the freeze-dried TATAPA and TAPA hydrogels were immersed in excess pure water at room temperature until equilibrium (Fig. 2a). TATAPA hydrogels reached a swelling equilibrium at 48 h and showed a swelling percentage at a range from 150% to 250%. In the meantime, the ultimate swelling ratio of TATAPA-3 hydrogel was much lower than TATAPA-1 and TATAPA-2,
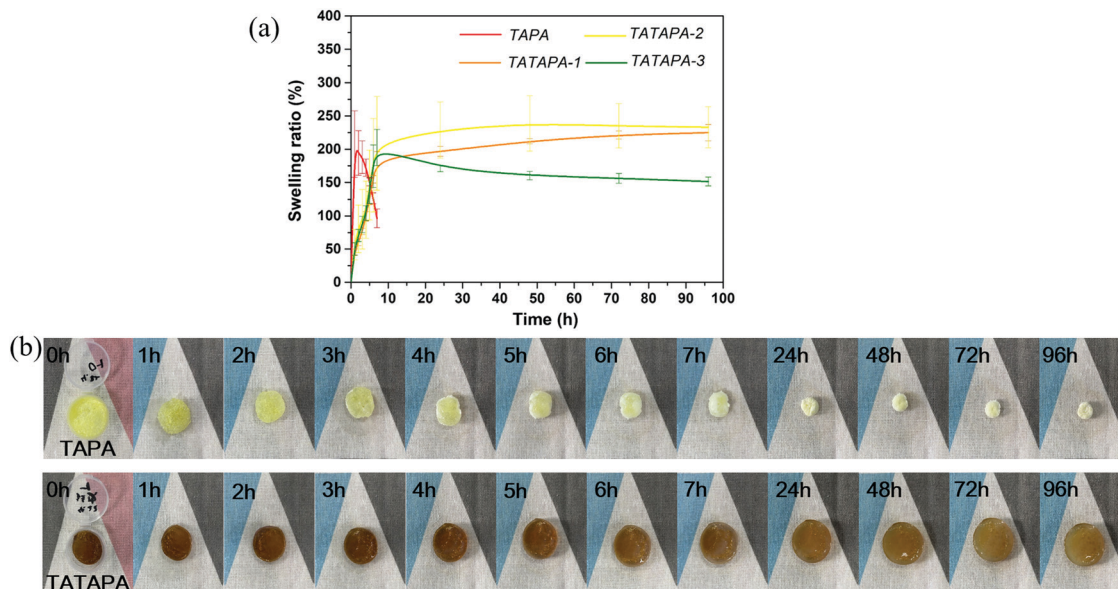
Fig. 2 (a) Swelling ratios of the TAPA, TATAPA-1, TATAPA-2 and TATAPA-3 hydrogels as a function of time. (b) Photos of the TAPA and TATAPA-2 hydrogels at different swelling times.

which could be ascribed to the increasing crosslinking density generated by the ascending amount of tannic acid. The TATAPA hydrogels were able to tolerate water immersion without dissociation for a month. In contrast, the TAPA hydrogel reached a maximum swelling ratio of 200% at 1 h and then lost weight gradually as time went by. The weight loss of the APA hydrogel was approximately 50% at 96 h, which demonstrated the supramolecular nature of this poly(thioctic acid)–phytic acid composite (Fig. 2b). The stretchability and mechanical strength were characterized by the tensile test. It could be inferred from the stress–strain curves that adding tannic acid was irrelevant to the tensile strength (2.5–3.0 kPa). However, when the dosage of tannic acid reached 1 g, it would introduce much impact on the breaking elongation (Fig. S4, ESI†). The average breaking elongation of the TATAPA-3 hydrogel reached 500%, which was the highest in contrast to the others. It should be noted that the TAPA hydrogel was too soft to obtain tensile mechanical parameters.

3.3. Adhesive properties

The TATAPA hydrogel could adhere to various daily used materials including rubber, glass, metal, stone, chrysanthemum, pigskin, wood and plastic. Prior to the above adhesive operations, the hydrogel patches could adhere to the bottom surface of a reagent rack (Fig. 3a and b). Furthermore, this kind of hydrogel was wearable and readily peeled off from the skin without lagging behind (Movies S1 and S2, ESI†). Therefore, the usage of TATAPA hydrogel instead of the ordinary band-aid would alleviate the pain caused by the patch removal. To quantify the adhesive force between the TATAPA hydrogel and versatile substrates, a lap-shear test was conducted (Fig. 3c and d). The adhesive strength was 11.7 kPa for wood, 8.8 kPa for poly(vinyl chloride) (PVC) chip, 8.6 kPa for a glass slide, 7.4 kPa

for a ceramic piece, 7.2 kPa for an aluminum chip and 5.9 kPa for a silicon rubber piece. The adhesion forces for poly(tetrafluoroethylene) (PTFE) and pigskin were relatively low, which was 2.3 kPa and 1.6 kPa, respectively. These results were in accordance with the choice of PTFE material as molds as well as the phenomenon that the TATAPA hydrogel could be comfortably peeled off from the skin. The adhesive strength of TATAPA hydrogel might be restricted by its tensile strength. With an aim to study the adhesive strength of the TATAPA hydrogel after dehydration, all the substrates except porcine skin were adhered to the TATAPA-2 hydrogel and then subjected to continuous heating at 60 °C for 8 h. It turned out that the dried TATAPA hydrogel showed enhanced adhesive strength in contrast to that of the previous measurement (Fig. S5, ESI†). Especially, the wood substrate could drain the water out of the TATAPA hydrogel. Moreover, the porous structure of wood was beneficial to increasing the hydrogel adhesive area. As a result, the adhesive strength for wood was 0.25 MPa on average, which was 25 times higher than that of the slowly dried hydrogel. The adhesive strength of other substrates also increased 2–5 times. These phenomena could be ascribed to enhanced interfacial supramolecular interactions during water evaporation. The adhesive strength of the TAPA and TATAPA hydrogel patches was also evaluated by the bursting pressure test (Fig. 3e, f and Fig. S6, ESI†). The bursting pressure of all hydrogels was similar to a range from 3.7 to 4.0 kPa after 5 min of intestine membrane adhesion. Moreover, the TATAPA hydrogel showed potential as a waterproof tape for broken rubber water pipes just after 5 min adhesion (Fig. 3g). The mended water pipe functioned normally after hydrogel adhesion for 24 h, which manifested the long-term use of TATAPA hydrogels even under a slowly dried conditions at room temperature (Movie S3, ESI†).
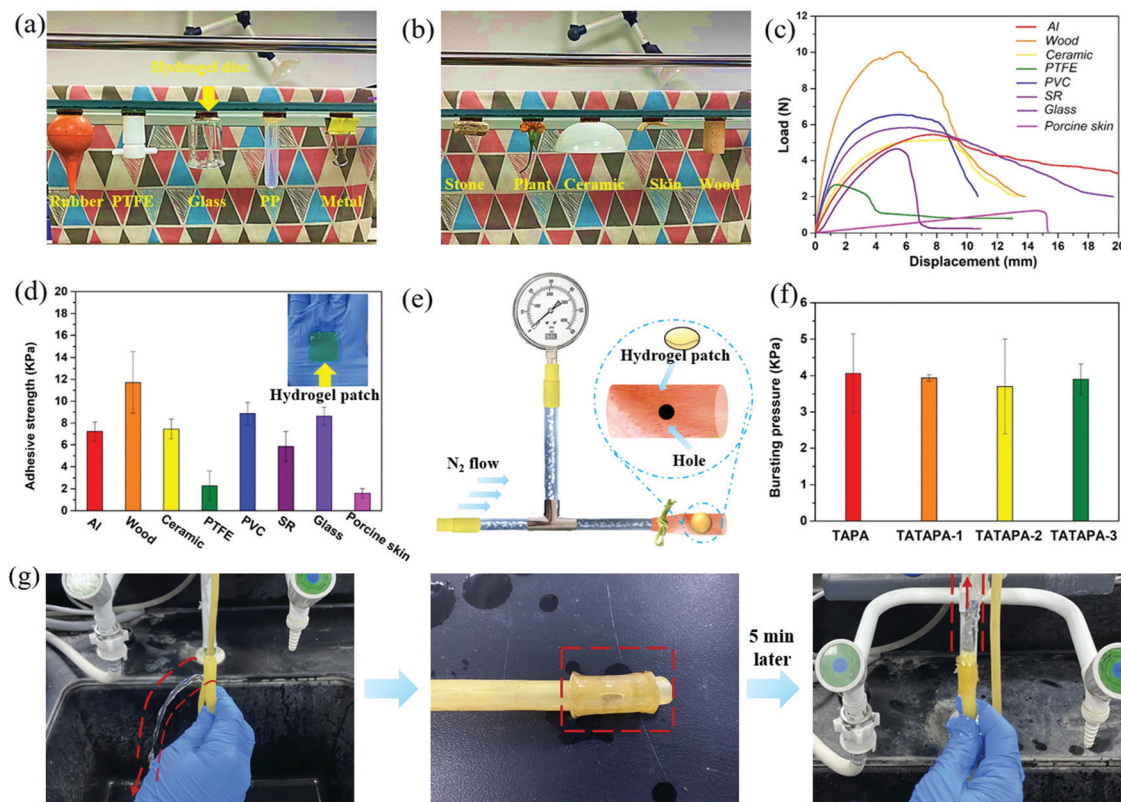
Fig. 3 Adhesive properties of the TATAPA hydrogels. (a) Image of adhesion between the TATAPA hydrogel (24 mm in diameter, 4 mm thickness) and a rubber ball, PTFE plug, glass beaker, PP centrifugal tube and metallic book clip. (b) Image of adhesion between the TATAPA hydrogel (24 mm in diameter, 4 mm thickness) and stone, a flower, a ceramic bowl, pigskin and wood. (c) Representative load–displacement curves of the TATAPA-2 patch (25 mm width, 25 mm length, 1 mm thickness) with various daily used substrates. (d) Adhesive strength of the TATAPA-2 hydrogel with different substrates. (e) Schematic illustration of the bursting pressure test. (f) Results of the bursting pressure test. (g) Images showing the ability of the TATAPA-2 hydrogel patch (24 mm in diameter) to mend a hole (5 mm in diameter) in a rubber water pipe.

Together with the adhesive results, the TATAPA hydrogel demonstrated universal adhesive properties to versatile hydrophobic and hydrophilic substrates, which could be ascribed to the polyphenol-based adhesive binding as well as the adhesive nature of poly(thioctic acid). Considering the fact that the chemical structure contained numerous pyrogallol and carbonyl groups, the hydrogel intended to adhere to various surfaces by supramolecular binding such as hydrogen bonding, hydrophobic interactions and π–π interactions, or by covalent bonding originating from quinone-based chemistry when tannic acid residues were oxidized.[53,54] Therefore, the TATAPA hydrogel might be promising in wound dressing as well as preventing superficial trauma bleeding with a long-term aid.

3.4. Rheology of the TATAPA hydrogels

The rheological properties of the TAPA and TATAPA hydrogels were also studied. The TATAPA hydrogel had self-healing properties and the restructured hydrogel was also stretchable after two gel pieces joined together for 2 h (Fig. 4a), which resulted from the dynamic hydrogel bonding between phosphate moieties and carbonyl moieties. The self-healing property of the TATAPA hydrogel was also viewed by repeated dynamic strain step testing (Fig. 4b). A 200% strain could result in a

sharp decrease of G' and G''. However, the hydrogel network remained stable since $G' > G''$. The hydrogel network was reconstructed since G' was maintained constant around 2200 Pa when γ returned to 1%. In the strain-sweep test, all TATAPA hydrogels had higher storage modulus (G') and loss modulus (G'') values than those of the TAPA hydrogel (Fig. 4c). The G' values of TATAPA hydrogels were almost nine times as much as those of the TAPA hydrogel, which could be ascribed to the enhanced stability of the hydrogel network after chemical crosslinking between tannic acid and thioctic acid. However, the ascending addition amount of tannic acid did not further increase G' values, manifesting that the mechanical reinforcement of tannic acid was limited. The tannic acid-crosslinked poly(thioctic acid) segments, which is the main component of the TATAPA hydrogel, played a critical impact on the rheological properties. Thus, linear regions between 0.1% and 100% were observed with $G' > G''$ for all the hydrogels. In contrast to our previous study on tannic acid–thioctic acid hydrogel,[48] the G' value of the TATAPA hydrogel increased nearly fourfold, revealing the contribution of PA-induced hydrogen bonding in mechanical reinforcement. Considering the results from the tensile test, it could be inferred that the hydrogel network remained stable under external force with no shear–thinning
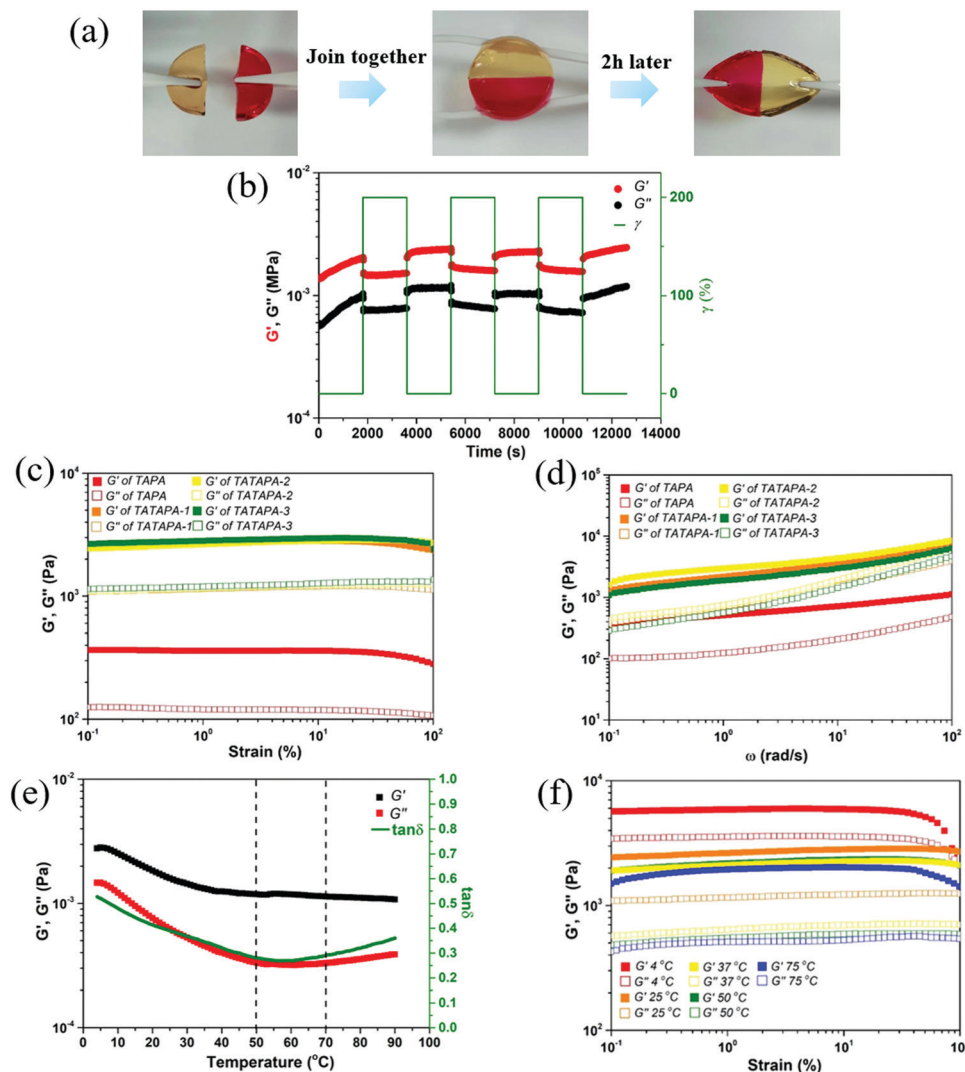
Fig. 4 Rheology of the TAPA and TATAPA hydrogels. (a) The self-healing property of the TATAPA hydrogel; half piece of the hydrogel was stained by Rh B. (b) Repeated dynamic strain step testing (γ = 200% or 1%, ω = 10 rad s^{-1}) on the self-healing property of the TATAPA-2 hydrogel at room temperature. (c) Strain-sweep measurements of the hydrogels with different thioctic acid/tannic acid molar ratios (25 °C, ω = 10 rad s^{-1}). (d) Frequency-sweep measurements of the hydrogels with different thioctic acid/tannic acid molar ratios (25 °C, γ = 1%). (e) Temperature sweep of the TATAPA-2 hydrogel; the heating rate was 1 °C min^{-1} (ω = 10 rad s^{-1}, γ = 1%). (f) Strain-sweep measurements of the TATAPA-2 hydrogel under different temperatures (4, 25, 37, 50, 75 °C, ω = 10 rad s^{-1}).

effect. The frequency-sweep of the hydrogels also showed the same tendency as the strain-sweep test (Fig. 4d). A temperature-sweep was also involved in studying the thermal sensitivity of the TATAPA-2 hydrogel (Fig. 4e). In the temperature range from 4 °C to 50 °C, tan δ decreased from 0.52 to 0.28. G' and G'' were maintained relatively stable at 50–70 °C. Subsequently, a small increase in tan δ from 0.28 to 0.36 was observed when the hydrogel was further heated to 90 °C. The dissociation of hydrogen bonding among carbonyl groups was accounted for the increased tan δ at the first stage (4–50 °C), which decreased inter-molecular interactions. Considering the multidentate supramolecular interaction provided by phytic acid, the temperature-sweep plateau at the second stage (50–70 °C) resulted from the retained hydrogen bonding between carbonyl

groups and phosphate groups. At the third stage (70–90 °C), dynamic disulfide exchange played a critical role and the S–Ar-based covalent crosslinking within the hydrogel resisted gel–sol transition (Scheme 2). Over the entire temperature range, the G' values were higher than the G'' values since the hydrogel should have a viscous behavior and its network remained stable under heating. The strong dependence of the rheological properties on temperature allows the TATAPA hydrogel to maintain shape stability as well as mold to the desired shape through the heating–cooling procedure, which is a typical feature of the supramolecular bulk hydrogels. Strain-sweep measurements at different temperatures demonstrated similar results, in which the hydrogel showed maximum mechanical strength at 4 °C (Fig. 4f). Moreover, in accordance with the temperature-sweep,
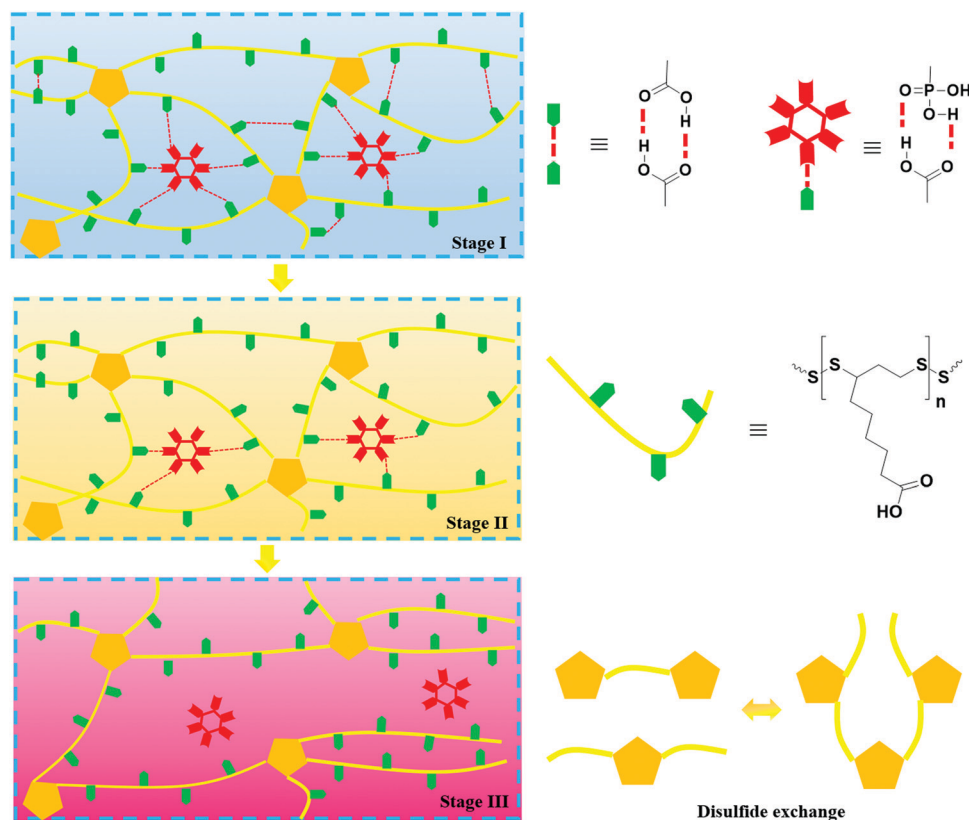
Scheme 2 The proposed dynamic bonds of the TATAPA hydrogel during the temperature sweep.

the G' values had negligible differences at 37 °C, 50 °C and 75 °C.

3.5. Antioxidant activity and cellular toxicity of TATAPA hydrogels

The antioxidant activity of the hydrogels was also evaluated by a DPPH radical assay. The scavenging capability of DPPH radical is a common method for measuring polyphenol-based oxidation resistance. The DPPH scavenging activity of all the TATAPA hydrogels after 10 min incubation with DPPH solution was 90%, which was far more than that of the TAPA hydrogel (Fig. S7, ESI†). The DPPH ethanol solution gradually changed color from dark violet to pale yellow when DPPH radicals were neutralized. It could be inferred that tannic acid residues in TATAPA hydrogels had a far-reaching positive effect on DPPH radical trapping, whereas a proportion of PA possessed a weak DPPH-scavenging capacity. *In vitro* cytotoxicity assay study of TATAPA-2 hydrogel with L929 cells was also performed since these kinds of cells are recognized as beneficial for wound healing (Fig. S8, ESI†). In the prospect of DAPI staining at certain time intervals, cell proliferation could be observed and the cell number in the hydrogel extracts tripled on day 2 and day 3 in comparison with that on day 1. Moreover, in contrast, to the blank control, the TATAPA hydrogel group exhibited a 2-time magnification of the cell number. These results demonstrated that the hydrogel possessed good biocompatibility, which could be applied as a wound dressing for multiple uses.

3.6. Utilization of TATAPA hydrogels as wound dressings

In vivo antibacterial ability of the TATAPA hydrogel was assessed by a burn MRSA infection model. A burn wound was made on the back of a pathogen-free BALB/c immune-competent male mouse by pressing a hot brass cylinder (90 °C) for 6 s and then inoculating with MRSA (Fig. 5a). Mice with burn wounds were treated with saline, TAPA hydrogel and TATAPA hydrogels, respectively. TATAPA and TAPA hydrogels could be directly pasted onto the wound sites. As a result, obvious recovery of MRSA-infected burn wound sites could be observed after removal of the TATAPA hydrogel patch after 72 h treatment. Whereas the other two groups had obvious redness and swelling appearance at the wound sites (Fig. 5b). H&E staining was also involved in assessing the degree of infection as well as the recovery status at the wound sites (Fig. 5c). After 24 h treatment, non-continuous or porous epidermal layers with large number of inflammatory cells (stained blue) existed in the saline and TAPA controls. In comparison with the other two groups, fewer inflammatory cells were found in the TATAPA group. After 72 h of treatment, the degree of ulceration of skin tissue deepened in the saline and TAPA controls with large disconnections in the epidermal layers. Nonetheless, an almost intact epidermis structure with a few inflammatory cells was observed in the TATAPA group, which showed that the TATAPA hydrogel reduced the inflammatory effects at the MRSA-infected burn wound site. Moreover, the bacterial burden of the wound sites was quantified by counting colony numbers on
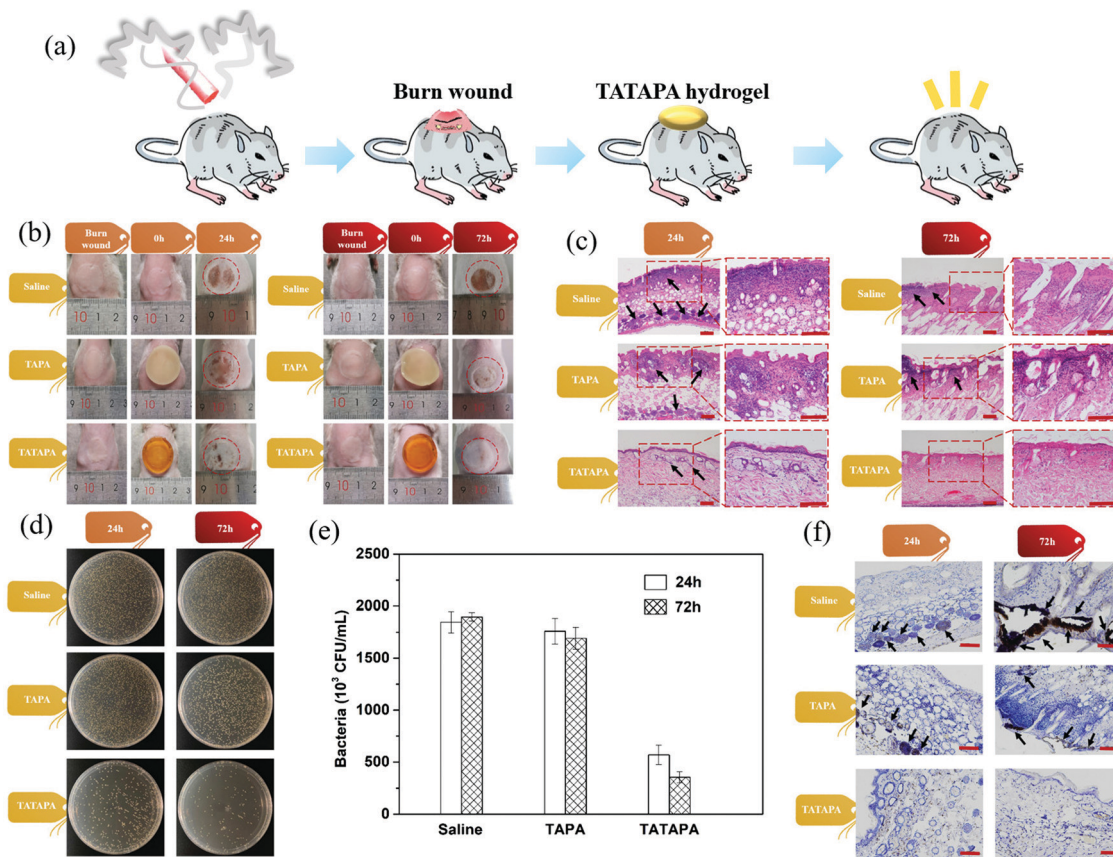
Fig. 5   *In vivo* anti-MRSA assay of hydrogels in a BALB/c mice burn wound model. (a) Schematic illustration of the mice with a burn wound treated with the TATAPA hydrogel for wound healing. (b) Images of the recovery status of the MRSA-infected mice treated with saline, TAPA hydrogel and TATAPA-2 hydrogel. (c) Histological analysis of wound tissue sections using H&E staining (inflammatory cells: black arrows; scale bar = 100 μm). (d) Photos of the bacterial colonies originating from the burn wound sites. (e) Quantitative evaluation of the bacterial burden (CFU mL^{-1}) from the infected wound sites treated with saline, TAPA hydrogel, and TATAPA-2 hydrogel at days 1 and 3 (n = 3). (f) Histological analysis of wound tissue sections using histochemical immunostaining (scale bar = 100 μm).

LB agar plates after 24 h and 72 h treatment, respectively (Fig. 5d and e). MRSA grew rapidly in burn wounds treated by saline and the TAPA hydrogel, and the number of bacteria was up to 1.84×10^6 CFU mL^{-1} and 1.76×10^6 CFU mL^{-1}, respectively. In contrast, the bacterial number in the TATAPA group was 5.69×10^5 CFU mL^{-1}, which was 1/3 of those from the control groups. After 72 h treatment, no further alleviation of bacterial burden could be observed in the saline and TAPA control groups. However, the number of bacteria was further reduced to 3.54×10^5 CFU mL^{-1} in the TATAPA group, which significantly reduced 80% bacterial burden. The determination of IL-1β expression *via* immunohistochemistry was also conducted since IL-1β plays a critical role in the protection against the mucosal pathogen *Staphylococcus aureus*.[55] In comparison with the saline and TAPA controls, continuous tissue with a lower degree of IL-1β expression (stained brown) was observed in the TATAPA group at 72 h post-treatment (Fig. 5f). All the above-mentioned results indicated that the TATAPA hydrogel had therapeutic effectiveness for the MRSA-infected burn wound sites, in which the proportion of tannic acid played a critical role. Moreover, the treatment of the TATAPA hydrogel

patch was simple with a facile removal property, which was desirable for emergency management of the epidermal wound.

3.7. TATAPA hydrogels for hemostasis

Hydrogel with hemostatic effect not only controls bleeding but also keeps the wound moist for wound healing. A common feature of adhesive hydrogels for bleeding wounds relies on sealing wounds and accelerating hemostasis. Interfacial adhesion is mainly based on the reaction between the chemical active groups belonging to the hydrogel and the amino group in the protein of a given tissue.[56–59] The hemostatic effect of the TATAPA hydrogels was also studied using a rat femoral artery model. In detail, a syringe was used to puncture the femoral artery of the rat. Subsequently, a TAPA or TATAPA hydrogel patch with 2 mm thickness was pasted onto the bleeding site (Fig. 6a). For the blank control group without any treatment, the blood loss at 90 s reached 57 mg and the hemostasis time overpassed 10 min (Fig. 6b). It could be observed through the transparent TATAPA-1 hydrogel path that the bleeding blood stagnated at the hydrogel/tissue interfaces and this stagnant blood volume no longer increased after 3–4 min adhesion,
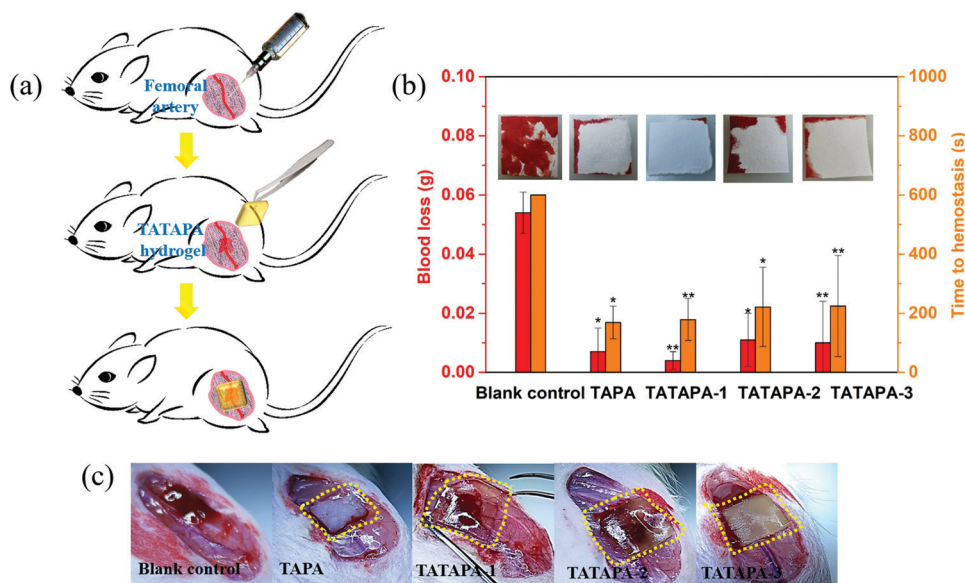
Fig. 6 The hemostatic effect of the TATAPA hydrogel. (a) Schematic illustration of TATAPA hydrogel treatment. (b) Blood loss of the SD rat femoral artery model during 90 s hydrogel patch treatment and the time to hemostasis ($n = 4$, $*P < 0.05$, $**P < 0.01$). (c) Images of the bleeding femoral artery treated with hydrogel patches at 90 s since adhesion.

Fig. 7 The hemostatic effect of the TAPA and TATAPA hydrogels in a liver hemostasis model of SD rats. (a) Images of the injured liver bleeding treated with different methods. (b) The accumulated blood loss from liver bleeding of SD rats treated with different methods ($n = 4$, $*P < 0.05$, $**P < 0.01$).

revealing that the hydrogel tightly and seamlessly sealed the bleeding site (Fig. 6c). In contrast, the TATAPA-1 hydrogel patch demonstrated the best hemostatic performance and the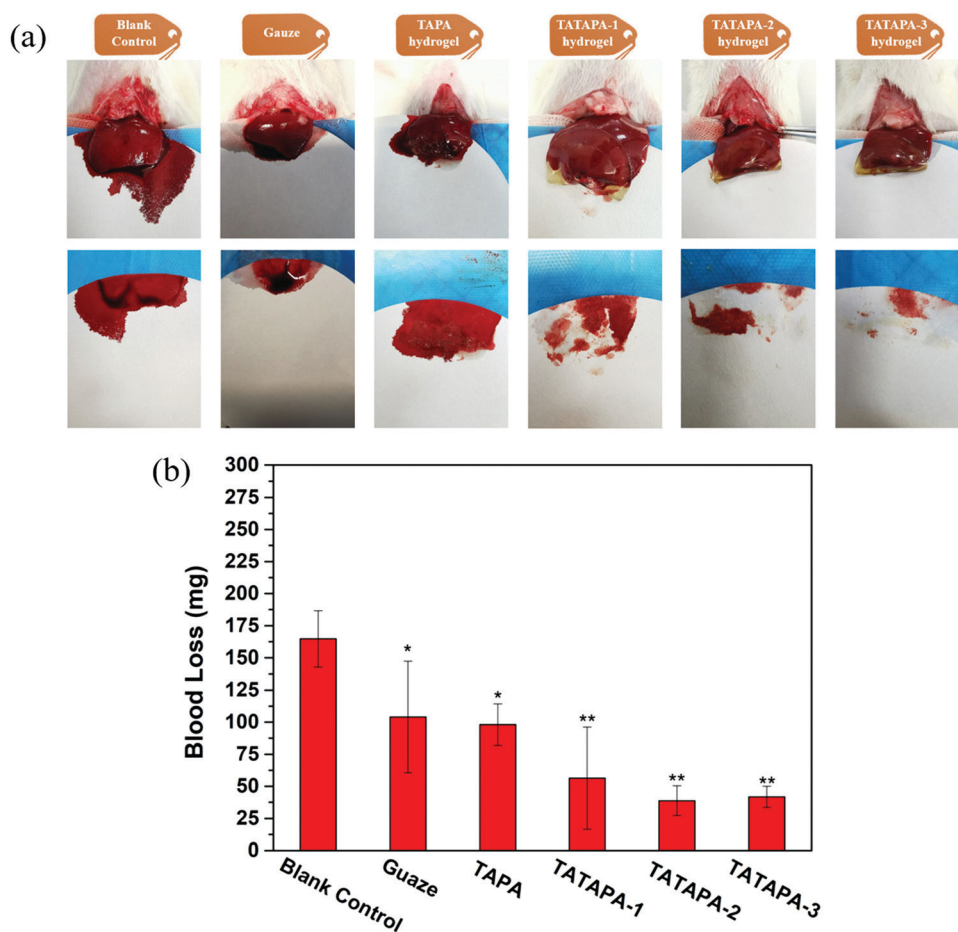 average blood loss at 90 s was only 4 mg (Movie S4, ESI†). However, the hemostatic effect of TATAPA-2 and TATAPA-3 hydrogels did not meet expectations in comparison with that of the TATAPA-1 hydrogel, in which the large proportion of tannic acid within hydrogels sacrificed adhesion capability as well as molecular flexibility by supramolecular interactions. Overall, the adhesion layer formed between the hydrogel patch and bleeding site could act as a physical barrier to prevent blood from leaking out thanks to polyphenol-based adhesion as well as the multi-carbonyl poly(thioctic acid). To further study the *in vivo* hemostatic effect of the hydrogels, a model of the liver bleeding of SD rats was established, in which a part of the rat's liver lobe was sheared off to simulate severe trauma. The liver wound without any treatment was used as a negative or blank control, whereas gauze pressing was used as a positive control. Moreover, both TAPA and TATAPA hydrogel patches were applied as hemostatic materials (Fig. 7a). In the case of the blank control group, massive hemorrhage from the cut section could be observed, causing a vast area of bloodstain on the filter paper. TATAPA-1, TATAPA-2 and TATAPA-3 hydrogels manifested desired hemostatic effect and the hemostatic efficiencies were 66%, 76% and 75%, respectively (Fig. 7b and Movie S5, ESI†). Typically, the TATAPA hydrogels could provide a broad bandage to the cut surface of the liver by tissue adhesion, which resisted further blood loss. In contrast, the gauze pressing treatment only achieved a hemostatic efficiency of 37%. The TAPA hydrogel turned out to be less effective than the TATAPA hydrogels since the absence of polyphenol-based adhesion. All the hemostatic tests showed that the TATAPA hydrogel could be applied in muscular artery hemostasis, in which the hydrogel sealed up the bleeding site by polyphenol-poly(thioctic acid)-based tissue adhesion. With an aim to test the biodegradability as well as the biocompatibility of the TATAPA hydrogel, a TATAPA-2 hydrogel disc (5 mm in diameter, 2 mm thickness) was implanted in a full-thickness skin wound of a male SD rat. The hydrogel exhibited a fast degradation behavior and the hydrogel disappeared on day 3 after implantation (Fig. S9a, ESI†). H&E stained sections of the tissue showed gradual subcutaneous tissue growth without an exaggerated immune response from day 1 to day 7. Both the *in vitro* and *in vivo* assays demonstrated that the hydrogel had desirable antibacterial properties, oxidation resistance, tissue adhesion performance, and good biocompatibility, which was appropriate for wound dressings, especially at superficial lesion locations.

4. Conclusion

To sum up, the TATAPA hydrogel was synthesized *via* a bottom-up method, in which both tannic acid and phytic acid acted as crosslinkers for the hydrogel network, which met our aim to develop a multifunctional adhesive gel free of toxic crosslinkers, oxidants, or heavy metal ions. The hydrogel was

transparent, moldable and wearable with a tensile strength of 2.5–3.0 kPa, a breaking elongation of 300–500% and a low swelling ratio of 200%. The adhesive test showed that TATAPA hydrogel had a universal adhesive property for various materials such as wood, glass, aluminum, ceramic and so on. Though the adhesion force towards skin tissue was relatively low, the TATAPA hydrogel was readily available for removal on demand and could be used even under a slowly dried condition. *In vivo* MRSA burn wound assay demonstrated that the hydrogel could relieve 80% bacterial burden with desirable recovery status after 3 day treatment in contrast to the controls. The hemostatic effect of the hydrogels was also studied by a rat femoral artery model, which revealed that the blood loss could be reduced to 4 mg at the 90 s since the hydrogel patch pasting and the hemostasis time was 3–4 min. Therefore, the TATAPA hydrogel is promising for scale-up production and can be used as a first-aid bandage for superficial lesion location in practical uses.

Conflicts of interest

The authors declare that they have no conflicts of interest. The tested people who wore TATAPA hydrogel in Fig. 1, Movies S1 and S2 (ESI†) were the first corresponding authors and this operation were approved by all the authors in this article.

Acknowledgements

References

1 K. Las Heras, M. Igartua, E. Santos-Vizcaino and R. M. Hernandez, *J. Controlled Release*, 2020, **328**, 532–550.
2 G. Xu, Y. L. Lu, C. Cheng, X. Li, J. Xu, Z. Y. Liu, J. L. Liu, G. Liu, Z. H. Shi, Z. T. Chen, F. N. Zhang, Y. X. Jia, D. F. Xu, W. Yuan, Z. Cui, S. S. Low and Q. J. Liu, *Adv. Funct. Mater.*, 2021, **31**, 2100852.
3 E. Y. Jeon, B. H. Hwang, Y. J. Yang, B. J. Kim, B. H. Choi, G. Y. Jung and H. J. Cha, *Biomaterials*, 2015, **67**, 11–19.
4 N. Annabi, K. Yue, A. Tamayol and A. Khademhosseini, *Eur. J. Pharm. Biopharm.*, 2015, **95**, 27–39.
5 N. Annabi, A. Tamayol, S. R. Shin, A. M. Ghaemmaghami, N. A. Peppas and A. Khademhosseini, *Nano Today*, 2014, **9**, 574–589.
6 H. Yuk, B. Lu and X. Zhao, *Chem. Soc. Rev.*, 2019, **48**, 1642–1667.

7   D. Caccavo, S. Cascone, G. Lamberti and A. A. Barba, *Chem. Soc. Rev.*, 2018, **47**, 2357–2373.

8   T. Xie, J. Ding, X. X. Han, H. Z. Jia, Y. Yang, S. Liang, W. X. Wang, W. G. Liu and W. Wang, *Mater. Horiz.*, 2020, **7**, 605–614.

9   B. K. Sun, Z. Siprashvili and P. A. Khavari, *Science*, 2014, **346**, 941–945.

10 W. Zhang, R. Wang, Z. Sun, X. Zhu, Q. Zhao, T. Zhang, A. Cholewinski, F. K. Yang, B. Zhao, R. Pinnaratip, P. K. Forooshani and B. P. Lee, *Chem. Soc. Rev.*, 2020, **49**, 433–464.

11 A. Jayakumar, V. K. Jose and J. M. Lee, *Small Methods*, 2020, **4**, 1900735.

12 Y. Shi, J. Zhang, L. Pan, Y. Shi and G. Yu, *Nano Today*, 2016, **11**, 738–762.

13 G. Fu, X. Yan, Y. Chen, L. Xu, D. Sun, J. M. Lee and Y. Tang, *Adv. Mater.*, 2018, **30**, 1704609.

14 F. F. Sun, Y. Z. Bu, Y. R. Chen, F. Yang, J. K. Yu and D. C. Wu, *ACS Appl. Mater. Interfaces*, 2020, **12**, 9132–9140.

15 H. L. Fan, J. H. Wang and Z. X. Jin, *Macromolecules*, 2018, **51**, 1696–1705.

16 Y. Y. Zheng, Y. Q. Liang, D. P. Zhang, X. Y. Sun, L. Liang, J. Li and Y. N. Liu, *ACS Omega*, 2018, **3**, 4766–4775.

17 M. S. Ma, Y. L. Zhong and X. L. Jiang, *Carbohydr. Polym.*, 2020, **236**, 116096.

18 J. H. Wang, X. Y. Chen, Y. Zhao, Y. M. Yang, W. J. Wang, C. Wu, B. Z. Yang, Z. T. Zhang, L. S. Zhang, Y. Liu, X. C. Du, W. F. Li, L. Qiu, P. J. Jiang, X. Z. Mou and Y. Q. Li, *ACS Nano*, 2019, **13**, 11686–11697.

19 W. W. Niu, Y. L. Zhu, R. Wang, Z. Y. Lu, X. K. Liu and J. Q. Sun, *ACS Appl. Mater. Interfaces*, 2020, **12**, 30805–30814.

20 G. K. Jani, D. P. Shah, V. D. Prajapati and V. C. Jain, *Asian J. Pharm. Sci.*, 2009, **4**, 308–322.

21 M. Ali and Q. Husain, *Int. J. Biol. Macromol.*, 2018, **116**, 463–471.

22 Y. Q. Zheng, Y. Luo, K. Feng, W. D. Zhang and G. J. Chen, *ACS Macro Lett.*, 2019, **8**, 326–330.

23 C. Y. Cui, C. C. Fan, Y. H. Wu, M. Xiao, T. L. Wu, D. F. Zhang, X. Y. Chen, B. Liu, Z. Y. Xu, B. Qu and W. G. Liu, *Adv. Mater.*, 2019, **31**, 1905761.

24 J. L. Guo, B. L. Tardy, A. J. Christofferson, Y. L. Dai, J. J. Richardson, W. Zhu, M. Hu, Y. Ju, J. W. Cui, R. R. Dagastine, I. Yarovsky and F. Caruso, *Nat. Nanotechnol.*, 2016, **11**, 1105–1111.

25 F. Ni, P. Xiao, N. X. Qiu, C. Zhang, Y. Liang, J. C. Gu, J. Y. Xia, Z. X. Zeng, L. P. Wang, Q. J. Xue and T. Chen, *Nano Energy*, 2020, **68**, 104311.

26 J. Zheng, R. Fan, H. Q. Wu, H. H. Yao, Y. J. Yan, J. M. Liu, L. Ran, Z. F. Sun, L. Z. Yi, L. Dang, P. P. Gan, P. Zheng, T. L. Yang, Y. Zhang, T. Tang and Y. Wang, *Nat. Commun.*, 2019, **10**, 1604.

27 Y. X. Gao, J. Hao, Q. Yan, F. P. Du, Y. Ju and J. Hu, *ACS Appl. Mater. Interfaces*, 2018, **10**, 17352–17358.

28 Q. Zhang, C. Y. Shi, D. H. Qu, Y. T. Long, B. L. Feringa and H. Tian, *Sci. Adv.*, 2018, **4**, eaat8192.

29 R. Wang, X. X. Wang, Y. J. Zhan, Z. Xu, Z. Q. Xu, X. H. Feng, S. Li and H. Xu, *ACS Appl. Mater. Interfaces*, 2019, **11**, 37502–37512.

30 X. Q. Zhang, Z. Li, P. Yang, G. G. Duan, X. H. Liu, Z. P. Gu and Y. W. Li, *Mater. Horiz.*, 2021, **8**, 145–167.

31 Q. Dai, H. M. Geng, Q. Yu, J. C. Hao and J. W. Cui, *Theranostics*, 2019, **9**, 3170–3190.

32 H. M. Geng, Q. Dai, H. F. Sun, L. P. Zhuang, A. X. Song, F. Caruso, J. C. Hao and J. W. Cui, *ACS Appl. Bio Mater.*, 2020, **3**, 1258–1266.

33 H. X. Mei, Z. L. Gao, K. J. Zhao, M. Q. Li, M. Ashokkumar, A. X. Song, J. W. Cui, F. Caruso and J. C. Hao, *Angew. Chem., Int. Ed.*, 2021, **60**, 21529–21535.

34 Y. Du, W. Z. Qiu, Z. L. Wu, P. F. Ren, Q. Zheng and Z. K. Xu, *Adv. Mater.*, 2016, **3**, 1600167.

35 C. Zhang, B. Wu, Y. Zhou, F. Zhou, W. Liu and Z. Wang, *Chem. Soc. Rev.*, 2020, **49**, 3605–3637.

36 D. E. Payne, N. R. Martin, K. R. Parzych, A. H. Rickard, A. Underwood and B. R. Boles, *Infect. Immun.*, 2013, **81**, 496–504.

37 J. Luo, J. Lai, N. Zhang, Y. Liu, R. Liu and X. Liu, *ACS Sustainable Chem. Eng.*, 2016, **4**, 1404–1413.

38 J. S. Guo, W. Sun, J. P. Kim, X. L. Lu, Q. Y. Li, M. Lin, O. Mrowczynski, E. B. Rizk, J. G. Cheng, G. Y. Qian and J. Yang, *Acta Biomater.*, 2018, **72**, 35–44.

39 X. C. Du, L. Wu, H. Y. Yan, L. J. Qu, L. N. Wang, X. Wang, S. Ren, D. L. Kong and L. Y. Wang, *ACS Biomater. Sci. Eng.*, 2019, **5**, 2610–2620.

40 W. Z. Qiu, G. P. Wu and Z. K. Xu, *ACS Appl. Mater. Interfaces*, 2018, **10**, 5902–5908.

41 J. Jing, S. F. Liang, Y. F. Yan, X. Tian and X. M. Li, *ACS Biomater. Sci. Eng.*, 2019, **5**, 4601–4611.

42 C. Chen, X. W. Geng, Y. H. Pan, Y. N. Ma, Y. X. Ma, S. Z. Gao and X. J. Huang, *RSC Adv.*, 2020, **10**, 1724–1732.

43 C. Chen, X. Yang, S. J. Li, F. J. Ma, X. Yan, Y. N. Ma, Y. X. Ma, Q. H. Ma, S. Z. Gao and X. J. Huang, *RSC Adv.*, 2021, **11**, 5182–5191.

44 J. J. Griebel, N. A. Nguyen, A. V. Astashkin, R. S. Glass, M. E. Mackay, K. Char and J. Pyun, *ACS Macro Lett.*, 2014, **3**, 1258–1261.

45 J. J. Griebel, S. Namnabat, E. T. Kim, R. Himmelhuber, D. H. Moronta, W. J. Chung, A. G. Simmonds, K. J. Kim, J. Van Der Laan, N. A. Nguyen, E. L. Dereniak, M. E. Mackay, K. Char, R. S. Glass, R. A. Norwood and J. Pyun, *Adv. Mater.*, 2014, **26**, 3014–3018.

46 Y. L. Liang, Z. L. Tao and J. Chen, *Adv. Energy Mater.*, 2012, **2**, 702.

47 C. X. Chai, Y. Y. Guo, Z. H. Huang, Z. Zhang, S. Yang, W. W. Li, Y. P. Zhao and J. C. Hao, *Langmuir*, 2020, **36**, 10448–10459.

48 C. Chen, X. Yang, S. J. Li, C. Zhang, Y. N. Ma, Y. X. Ma, P. Gao, S. Z. Gao and X. J. Huang, *Green Chem.*, 2021, **23**, 1794–1804.

49 K. H. Hong, *Polym. Bull.*, 2017, **74**, 2861–2872.

50 M. Xu, A. Khan, T. J. Wang, Q. Song, C. M. Han, Q. Q. Wang, L. L. Gao, X. Huang, P. Li and W. Huang, *ACS Appl. Bio Mater.*, 2019, **2**, 3329–3340.

51 R. Eelkema and A. Pich, *Adv. Mater.*, 2020, **32**, 1906012.

52 H. Wang, P. T. Zheng, H. Yi, Y. Y. Wang, Z. H. Yang, Z. W. Lei, Y. K. Chen, Y. H. Deng, C. Y. Wang and Y. Yang, *Macromolecules*, 2020, **53**, 8539–8547.

53 N. Li, X. Yang, W. Liu, G. H. Xi, M. S. Wang, B. Liang, Z. P. Ma, Y. K. Feng, H. Chen and C. C. Shi, *Macromol. Biosci.*, 2018, **18**, 1800209.

54 L. Han, K. Z. Liu, M. H. Wang, K. F. Wang, L. M. Fang, H. T. Chen, J. Zhou and X. Lu, *Adv. Funct. Mater.*, 2018, **28**, 1704195.

55 T. Shimada, B. G. Park, A. J. Wolf, C. Brikos, H. S. Goodridge, C. A. Becker, C. N. Reyes, E. A. Miao, A. Aderem, F. Gotz, G. Y. Liu and D. M. Underhill, *Cell Host Microbe*, 2010, **7**, 38–49.

56 Y. Q. Liang, Z. L. Li, Y. Huang, R. Yu and B. L. Guo, *ACS Nano*, 2021, **15**, 7078–7093.

57 B. L. Guo, R. N. Dong, Y. P. Liang and M. Li, *Nat. Rev. Chem.*, 2021, **5**, 773–791.

58 M. Li, Z. Y. Zhang, Y. P. Liang, J. H. He and B. L. Guo, *ACS Appl. Mater. Interfaces*, 2020, **12**, 35856–35872.

59 R. Yu, H. L. Zhang and B. L. Guo, *Nano-Micro Lett.*, 2022, **14**, 1.